JOURNAL OF OPTOELECTRONICS AND ADVANCED MATERIALS, Vol. 11, No. 8, August 2009, p. 1094 - 1099

Thermal and structural analysis of the crystallization dynamics of metallic glass - $Fe_{40}Ni_{38}B_{18}Mo_4$

H. THOMAS[a,b*], V. THOMAS[b], R. V. RAMANUJAN[c], M. R. ANANTHARAMAN[a]
[a]*Department of Physics, Cochin University of Science & Technology, Cochin 682 022, Kerala, India*
[b]*Department of Physics, Christian College, Chengannur 689 122, Kerala, India*
[c] *School of Materials Engineering, Nanyang Technological University, Singapore 639 798.*

Structural and crystallization kinetic studies of $Fe_{40}Ni_{38}B_{18}Mo_4$ alloy ribbons under non-isothermal conditions are reported. The present analyses have been focused on the peaks of the Differential Scanning Calorimetriy (DSC) curves and a detailed understanding about the kinetics of crystallization of the alloy. The activation energy of crystallization of 3.49 ± 0.22 eV/atom and 4.51 ± 0.21eV/atom and Avrami exponents of 1.22 and 1.39 were obtained for the primary and secondary crystallization steps. The alloy has a characteristic glass transition temperature of 648 K and super cooled liquid region spanning around 47 K. These values are correlated to the kinetics of phase transformations and microstructural modifications in the alloy with annealing. The structural evolution associated with temperature is also discussed.

(Received May 29, 2009; accepted July 29, 2009)

Keywords: Metallic Glasses A, Crystal Growth B, Enthalpy C, Kinetics C, Thermodynamic Properties C

1. Introduction

Recently there is renewed interest in metallic glasses due to their potential applications in metallurgy and soft magnetic devices. The presence of short-range order combined with the absence of crystal defects such as grain boundaries and dislocations make them cheap alternatives for various applications. Metallic glasses are usually synthesized by rapid quenching techniques with cooling rates often exceeding 10^6 K/s. Synthesis of nano-crystalline materials, derived from amorphous metallic glasses through thermal treatments, have opened up new vistas for tailoring the properties of these classes of materials [1,2]. The extreme magnetic softness exhibited by these alloys can be attributed to the averaging of anisotropies over grains and the balance between exchange correlation length and grain size. They exhibit ferromagnetism characterized by high saturation magnetization, vanishing macroscopic anisotropy, negligible magnetostriction and large magnetic permeability [3]. $Fe_{40}Ni_{38}B_{18}Mo_4$ is one such alloy that is widely used for sensor and soft magnetic applications. The material is reported to have two-stage crystallization as is usually the case with most Fe based metallic glasses [4].

Activation energy of crystallization is a pertinent parameter that decides the application potential of metallic glasses. Higher activation energies are desirable for soft magnetic applications while lower values are appropriate for data storage purposes. Heat treatment of metallic glasses can catalyze crystallization in the material by supplying thermal energies to overcome the activation energy for crystallization. The material devitrifies into a supersaturated solid solution which consequently decays into a mixture of solid solution and crystalline phase or phases [5]. In any material, crystallization proceeds through nucleation, subsequent growth and Oswald ripening and thus the crystallization process is primarily governed by thermodynamics as well as diffusivities of constituent atoms. All these stages have characteristic activation energies and without loosing generality one can combine the energy barriers for all these processes into a single activation energy E_c [6]. The approximation is warranted by the reasoning that for most of the materials these three stages has overlapping energy curves.

There are discrepancies between the activation energies E_c of different crystallization stages of $Fe_{40}Ni_{38}B_{18}Mo_4$ alloy reported by various investigators. Antonione et al [7] was the first to report the crystallization dynamics of the material. Using non-isothermal calorimetric studies he had reported two-stage crystallization with activation energies 3.07 eV/atom and 3.46 eV/atom respectively for the two phases. However Majumdar and Nigam [8] observed three stage crystallization in the material. Cubrera et al [9] had done a quantitative investigation on the crystallization kinetics and activation energies using both non-isothermal (2.984 and 3.678 eV/atom) and isothermal methods (2.984 and 4.673 eV/atom) using Differential Scanning Calorimetry (DSC), Differential Thermal Analysis (DTA) and resistivity. Nicolai [10] has found five-step crystallization in the sample. Su Jen [11] reported the activation energy for α-Fe to be 2.92 eV/atom, and for (Fe, Ni) B to be 3.85 eV/atom. The above discussion suggests that reports on the crystallization dynamics of $Fe_{40}Ni_{38}B_{18}Mo_4$ are rather scanty and there exists diverse opinions about the activation energies for the nucleation and phase separation.

Metallic glasses are considered to exhibit structural and chemical disorder because of the high quenching rate

involved in the fabrication process. In devitrification of metallic glasses, the nucleation rate sigmoidally increases from zero to an ultimate steady state value. Kolmogorow-Johnsn-Mehl-Avrami (KJMA) model replicate the nucleation rate with a sigmoidal curve and the model was widely used for evaluating Avrami exponent which signifies the dimensionality of crystal growth. Stanislav Kurajicaa et al [12] reported the *n* values for both the crystallization steps of $Fe_{40}Ni_{38}B_{18}Mo_4$ to be nearly equal to 2. However, according to S U Jen et al [11] the first stage has an *n* value of 2.92, and for second stage *n* = 3.85. Jen et al. reported the second stage to have two *n* values indicating the changes of kinetics of crystallization, with the former section with *n* = 3.5 that signifies nucleation with constant nucleation rate, while the latter section with *n* = 1.2 signifies growth by diffusion without nucleation.

From the above discussion it is evident that there have been diverse views about the kinetics of crystallization and crystallization stages of $Fe_{40}Ni_{38}B_{18}Mo_4$. In the present work we report the crystallization dynamics of $Fe_{40}Ni_{38}B_{18}Mo_4$ employing DSC, X-Ray Diffraction (XRD) and analysis methods like Kissinger and KJMA. A precise knowledge about the kinetics of crystallization is extremely important to determine the activation energy of crystal growth from DSC data. The present study employs techniques like DSC to establish the mechanism of crystallization and to evaluate the activation energy of crystallization and Avrami exponents.

2. Experimental methods

Alloy ribbons having the composition $Fe_{40}Ni_{38}B_{18}Mo_4$ were provided by Metglas Corporation. The as received ribbons were tested using XRD for their amorphous nature. The ribbons were 20 μm in thickness and 25 mm in width. The bulk ribbons were subjected to DSC with the aimto determine the crystallization temperatures and thermal stability. Based on the DSC results the ribbon samples were annealed at different temperatures ranging from 373 - 773 K under high vacuum conditions. The samples were subjected to the annealing temperature at a heating rate of 5K/min, kept there for one hour and cooled subsequently with the same ramp rate. The enthalpy change associated with the phase transformation is calculated by integrating the peak area. The activation energies of crystallization were determined using the Kissinger equations [13].

In the Kissinger Model, during an isothermal transformation subjected to an instantaneous isobaric change, the crystallization process is usually represented by the Avrami's equation

$$x(t) = 1 - e^{-(Kt^n)} \tag{1}$$

where *K* is the rate constant and *n* is the order parameter which incorporates the dimensionality of crystal growth. The rate constant obeys an Arrhenius type relation:

$$K = K_o e^{\left(-\frac{E_c}{k_B T}\right)} \tag{2}$$

According to Kissinger, equation (1) can be approximated as

$$\frac{dx}{dt} = (1-x)nK^n t^{n-1} \tag{3}$$

Expressing *t* in terms of *x* from equation (1) the rate of crystallization becomes

$$\frac{dx}{dt} = AnK(1-x) \tag{4}$$

where

$$A = \left[-\ln(1-x)\right]^{\frac{n-1}{n}} \tag{5}$$

However in non-isothermal crystallization the heating rate is assumed to be a constant and the relation between the sample temperature *T* and heating rate *b* can be written as

$$T = T_i + bt \tag{6}$$

where T_i is the initial temperature.

The time derivative of *K* can be evaluated using equations (2) and (6) as

$$\frac{dK}{dt} = \left(\frac{dK}{dT}\right)\left(\frac{dT}{dt}\right) = \left(\frac{bE_c}{RT^2}\right)K \tag{7}$$

Using equations (4) and (7), Kissinger has shown that

$$\ln\left(\frac{b}{T_p^2}\right) = -\frac{E_c}{RT_p^2} + C \tag{8}$$

where *C* is a characteristic constant of crystallization .

In this method the activation energy is determined by plotting $\ln\left(\frac{b}{T_p^2}\right)$ versus $\frac{1000}{T_p}$, the slope of the straight line fit gives $-\frac{E_c}{1000R}$ from which the E_c values were evaluated.

The kinetics of phase transformations is usually modeled using the well-known KJMA equation [14]. The equation predicts an “S type sigmoidal curve” for the transformation with slow rate of transformation at the beginning which then accelerates and there after decelerates. The volume fraction transformed = transformed volume/total volume: $f = V / V_{total}$. The KJMA equation is built on the basic assumption of random distribution of nuclei in the material. The theory predicts

that the volume fraction transformed is exponentially dependant on the absolute temperature.

$$x(t) = 1 - e^{[-(\kappa t)^n]} \tag{9}$$

where *n* is an integer or half integer that reflects the dimensionality and mode of nucleation and growth of crystals. *K* is the thermally activated reaction rate constant with Arrhenian type temperature dependence.

$$K = K_o e^{\left[-\frac{E_a}{RT}\right]} \tag{10}\backslash$$

E_c denotes the activation energy and K_o the frequency factor. At small times the equation reduces to:

$$X = (\kappa t)^n$$

and the derivative

$$\frac{d \ln X}{d \ln t},$$

gives the exponent *n*.

The above equations are extensively used for the kinetic analysis of materials from DSC data. The theoretical derivation makes the fundamental assumption that the sample is heated isothermally. However the theory is further applied to nonisothermal cases by assuming a constant heating rate, and that justifies its application for the analysis of Avrami exponents using nonisothermal DSC.

The X-ray diffraction (XRD) spectra of the pristine samples, as well as annealed were recorded using an X-ray diffractometer (Rigaku D-max-C) using Cu Kα radiation (λ=1.5405 Å). The average particle size is determined from the measured width of their diffraction curves using Scherer formula $D = \left(\frac{0.9\lambda}{\beta \cos\theta}\right)$, where β is full width at half maximum (FWHM), D the average grain size and θ the diffracting angle.

3. Results and discussion

3.1 Crystallization studies

The DSC of the as-prepared ribbon samples were conducted at constant heating rates of 5, 10, 20 and 25 °K min^{-1} to investigate the inherent thermodynamics governing the crystallization process (Fig. 1). The first crystallization peak inception occurs at T_1 = 699 K while the second one is at T_2 = 809 K (heating rate 15 K min^{-1}), and up to 900 K, on DSC trace, no other thermodynamic events were found which is the characteristic response showed by Fe rich amorphous alloy materials with low B content. However the small kink just before the first pertinent peak in the DSC trace at a heating rate 20 K min^{-1} can be ascribed to the structural relaxation, chemical ordering and glass transition in the material with thermal gradients. Hence, this indicates that the structure of this material, may have started to relax far below the crystallization temperature, is in a state very far from equilibrium because it has been produced by rapid quenching and has been stored at room temperature where scope for thermal relaxation is negligible. Further, glassy state is characterized by large viscosity and hence the relaxation kinetics is relatively sluggish leaving little scope for local atomic rearrangements. This type of thermal relaxation may be prominent near the glass transition temperature, which is revealed as an endothermic peak in the DSC spectrum due to change in specific heat. However, if the relaxation is fast, such an endothermic peak is manifested as a small dip due to a fast change in total heat content. The total heat content for this thermodynamic event is 11.8 J/g, which characterizes the surplus energy over the equilibrium alloy state. Relatively lower value of the enthalpy of structural relaxation compared to the enthalpy of crystallization of first and second crystallization steps is indicative of the near perfect glassy state and lower free volumes prevailing in this alloy. The endothermic peak becomes more prominent with higher temperature annealing, which can be accounted for by assuming that the as quenched sample is in a metastable equilibrium state. Annealing this glass with increasing heating rates stimulates a relaxation towards more stable state and, as a consequence, an excess enthalpy of relaxation is released at that temperature. The excess enthalpy is equal to the area enclosed by the kink and this area changes with heating rate since the dynamics of heat treatment is influential on shifting the peak crystallization temperature.

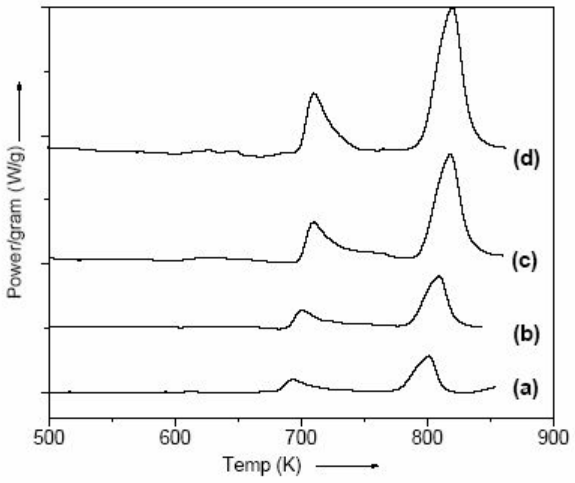

Fig. 1. DSC thermogram of metglas ribbons for heating rates (a) 5 K/min (b) 10 K/min. (c) 20 K/min. (d) 25 K/min.

The first peak, at low temperature, is due to the formation of crystallization phases including the metastable phases, which is rather sharp signifying spontaneous nucleation and grain growth and implies that

the delay between nucleation and grain growth is very small. This can be ascribed to the relative ease of expulsion of highly diffusive boron from the vicinity of FeNiMo clusters. The initial crystalline phase is responsible for the excellent magnetic properties exhibited by $Fe_{40}Ni_{38}B_{18}Mo_4$ [15]. The second phase with relatively low sharpness reflects languid nucleation and growth of the second phase at the expense of the first phase. The second peak in DSC exotherm corresponds to redistribution and re-crystallization of metastable phases of the residual amorphous phase and the precipitation of $FeNiMo_{23}B_6$ which is deleterious to the soft magnetic properties [16]. The first exotherm with its asymmetric end extended towards to the higher end of the spectrum can be attributed to the devitrification process giving a finely dispersed Fe-Ni-Mo nano-phase embedded in a residual boron rich amorphous matrix. Furthermore it is evident that the first crystallization step extends up to the initial stage of the second crystallization with progressive grain growth of the initially nucleated crystallites. The deconvolution of the first peak using Gaussian curve fitting reveals two distinct Gaussian curves instructive of the biphasic transitions at that regime. The enthalpy change associated with crystallization, which corresponds to the maximum energy, associated with the phase transformations for the two peaks in the primary crystallization step are 13.9 J/g and 17.71 J/g respectively. From the prominence of the first peak and in comparison with the reported literature on this material it can be concluded that the first phase corresponds to α -FeNiMo. However no other phases excepting FeNiMo are found in samples annealed up to 690 K, henceforth the second associated peak can be ascribed to transformation of primary crystallization products to more stable phases resulting from redistribution and structural rearrangement of α -FeNiMo phase.

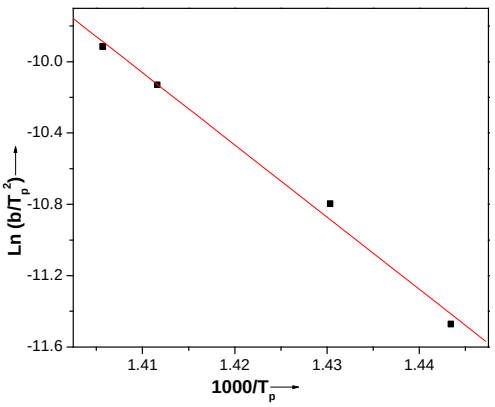

Fig. 2. Kissinger plot corresponding to the first peak in the DSC exotherm.

The second prominent peak in the DSC has a characteristic enthalpy of 51 J/g and this comparatively higher value shows higher annealing temperatures and high thermal energies for nucleation and growth. With progressive heating the crystallization in the sample starts at around T_x = 695 K and the peak fitting of the small dip in the DSC referring to relaxation yields the glass transition temperature T_g = 648 K. In our investigation we have determined the onset temperature T_g as the characteristic temperature which can be determined as the intersection of the tangents to the scan above and below the initial change in the baseline slope. Thus, the super cooled liquid region ΔT_x is estimated to be 47 K. The relatively higher value of $\Delta T_x = T_x - T_g$ explains the improved thermal intransigence of $Fe_{40}Ni_{38}B_{18}Mo_4$, which stems from the larger atomic size and the negative heat of mixing of alloying elements. A duplex structure in Fe-base hypo-eutectic alloys is possible as long as α-Fe nanoparticles expel a component that acts to raise the crystallization temperature of the remaining amorphous phase [17]. In this case one can infer that a good percentage of the heavy element Molybdenum having relatively larger size and higher negative heat of mixing get expelled from the crystalline matrix into the surrounding amorphous boron rich phase resulting in a duplex structure.

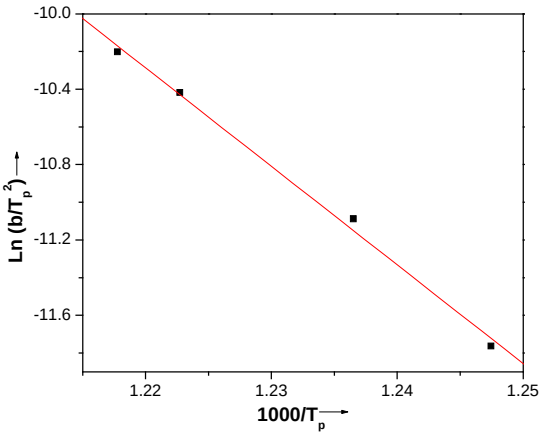

Fig. 3. Kissinger plot corresponding to the second peak in the DSC exotherm.

Fig. 2 and 3 shows the plots of $\ln b$ with $\frac{1000}{T_p}$ of $Fe_{40}Ni_{38}B_{18}Mo_4$ for the two crystalline phases. The activation energies are calculated from the slopes of the straight line fits. The activation energy calculated using the Kissinger model turns out to be 3.49 ± 0.22 eV/atom for the primary crystallization step and 4.51 ± 0.21 eV/atom for the second crystallization step.

3.2 Dynamics of crystal growth

Table 1 and 2 lists the values of the Avrami index *n* for three different heating rates. The data elucidates a clear decreasing trend of Avrami index with increasing heating rate for the second peak and a reverse trend for the first

peak. Slow heating rates were desirable for better completion of the crystallization process and stronger intergranular coupling. These slower heating rates therefore led to smaller effective magnetic anisotropies and better soft magnetic properties [17]. Avrami's analysis of nucleation and growth process leads to a value $n = 1.5$ if all the nuclei are present at time $t = 0$ and the subsequent growth of particles is parabolic. Heating rate of 5 K/min favors parabolic growth of crystallites and there is a clear trend for parabolic to circular growth of crystallites with increasing heating rates. It is well known that the crystallization of metallic glasses is associated with the nucleation and growth process, and the extent of crystallization increases with an increase in heating rate. In other words it tends to its maximum value. The decreasing trend of *n*, therefore, shows the decrease in the nucleation rate due to nucleation saturation. and that the character of crystallization goes over from nucleation-driven in the beginning to a growth-driven regime by the end of the crystallization process**.** [18]

Table 1. Table depicting the Avrami exponent for the primary crystallization step for various heating rates

K/min	II Peak temp (K)	*n*
5	528.63	1.58
10	535.55	1.37
20	544.84	1.22

Table 2. Table depicting the Avarami exponent for the secondary crystallization step for various heating rates

K/min	I Peak temp (K)	*n*
5	419.96	1.02
10	427.47	1.30
20	436.08	1.34

According to Christian [19], the Avrami exponent for the first phase with n = 3.5 signifies nucleation with constant nucleation rate, while the secondary phase with n = 1.2 signifies growth by diffusion without nucleation. This fact also agrees partially with investigation by other techniques that α-FeNiMo crystallites first grow in size and number, but then nucleation stops at the later stage of crystallization. However the assignment of $n = 3.5$ with the first stage of crystallization is fraught with error**.** This higher value for nucleation and growth in the alloy ribbon may be due to overlooking the presence of initial islands of compositional fluctuations in the alloy that can serve as nuclei for heterogeneous nucleation and growth during heating. During rapid quenching, some compositional fluctuation or even nuclei may be quenched in and a high quenching rate will reduce the size and number of such quenched-in nuclei reflecting in the Avarami exponent of the alloy [20]. For the first crystallization step the average value of *n* comes out to be 1.22, which shows that the crystallization mechanism in the present glasses has approximately one-dimensional growth during the amorphous to crystalline transformation. The values of the Avrami exponent, $n = 1$, are consistent with diffusion-controlled growth with a nucleation rate close to 0. We have observed the second stage to have only one *n* value corresponding to $n \sim 1.39$. This can be ascribed to the one dimensional growth of $FeNiMo_{23}B_6$ crystallites in the amorphous matrix.

3.3. X-ray diffraction studies on ribbons

XRD patterns shown in Fig. 4 and 5 illustrate the various phases present in quenched $Fe_{40}Ni_{38}B_{18}Mo_4$ ribbons as well as heat treated ones at different temperatures 625 and 773 K (around the first and the second crystallization peaks). The crests in as quenched samples are in harmony with the earlier reports on crystallization of metglas [8]. The amorphous peak in pristine sample can be attributed to FeNiMo solid solution. Evidence of the earlier assumption of the existence of a metastable state of metastable equilibrium for the quenched alloy is found in the x-ray diffraction pattern of the pristine alloy. The basic argument to support this assumption emerges from the fact that after annealing the glass at 625 K distinct Bragg peaks were noticeable. Using JCPDS database the peaks can be credited to primary crystallization product FeNiMo phase and a small volume fraction of $FeNiMo_{23}B_6$ with grain sizes of 10.24 nm. At 625K anneal almost 68% of the crystalline volume fraction were FeNiMo particles of size ~13.37 nm, substantiating the classification of $Fe_{40}Ni_{38}B_{18}Mo_4$ as a nano-crystalline soft magnetic alloy. Lower volume fractions ~32% of Boride phase with ~8.57 nm grain sizes ensures that the 625 K annealing sample exhibits good soft magnetic properties. However with augmented annealing temperatures, most of the crystalline volume fraction was $FeNiMo_{23}B_6$ phase with minute percentage of FeNiMo. At 773 K the volume fraction of FeNiMo and the size FeNiMo islands increases.

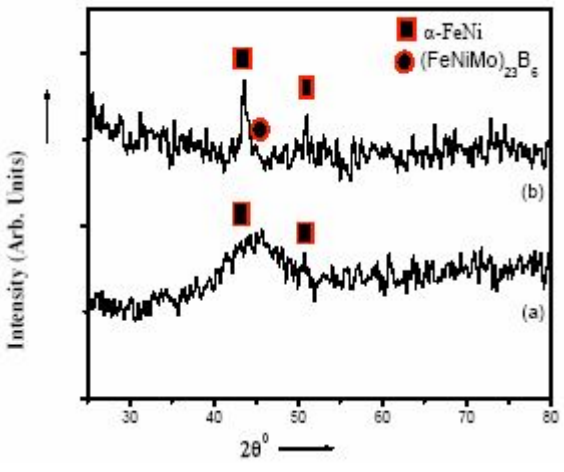

Fig. 4. XRD patterns of metglas ribbons (a) un-annealed (b) annealed at 773 K

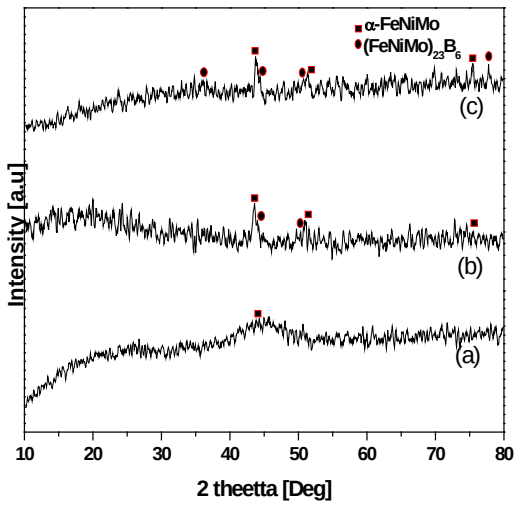

Fig. 5. XRD spectrum of metglas ribbons annealed at various temperatures. (a) Unannealed ribbon (b) annealed at 623 K (c) annealed at 773 K.

4. Conclusions

Metallic glass $Fe_{40}Ni_{38}B_{18}Mo_4$ shows glass transition, super cooled liquid region and sequential crystallization with progressive annealing temperatures. The kinetic parameters glass transition temperature T_g, the onset temperature of crystallization T_{x1}, super cooled liquid region defined as the temperature interval between T_g and T_x, and Avrami exponents for the alloy are measured and calculated and are found to be in partial agreement with existing reports. The heating rate dependence b on T_p is used to evaluate the activation energy of crystallization for the Fe-Ni-Mo and boride phases. The activation energies estimated using Kissinger method agrees fairly well with the existing reports. The large supercooled liquid region before crystallization may be ascribed to the unequal diffusivities of the constituent elements.

Acknowledgements

The authors wish to acknowledge the financial assistance received form Department of Science and Technology, New Delhi.

References

[1] R. Hesegava, R. C. ӦHandley, J. Appl. Phys. **50,** 1551 (1979).
[2] S. Shirae, J. Appl. Phys. **50** 7618 (1979).
[3] R. Hesagava, M. C. Narasimhan, N, Decristofara, J. Appl. Phys. **49** 1712 **(**1978).
[4] S. W. Du, R. V. Ramanujan, J. Meta. Nano. Mater. **23** 207 (2004).
[5] J. Li, Z. Su, T. M. Wang, S. Hage, H. Hahn, Y. Shirai, J. Mater. Sci. **34** 111 **(**1999).
[6] S. Ram, Cur. Sci. **86** 832 (2004).
[7] C. Antonione, L. Battezzati, A. Lucci, G. Riontino, G. Venturelo, Scripta Met. **12** 1011 (1978).
[8] K. Majumdar, A. K. Nigam, J. Appl. Phys. **51** 4218 (1980).
[9] F. L. Cumbrera, H. Miranda, A. Conde, R. Marquez, P. Vigier, J. Mater. Sci. **17** 2677 (1982).
[10] H. P. Nicolai, G. Kopmann, G. Frommeyer, Z. Metallkd. **72** 558 (1981).
[11] S. U. Jen, D. R. Huang, Chin. J. Phys. **24** 239 (1986).
[12] S. Kurajicaa, J. Schmauch, E. Tkaleca, Croatica Chemica Acta **75 (3)** 693 (2002).
[13] H. E. Kissinger, J. Res. Nat. Bur. Stand. **57** 217 (1956).
[14] D. R. Dos Santosa, D. S. Dos Santos, Mater. Res. **4-1** 47 **(**2001).
[15] T. Hysen, S. Deepa, S. Saravanan, R. V. Ramanujan, D. K. Avasthi, P. A. Joy, S. D. Kulkarni, M. R. Anantharaman, J. Phys. D: Appl. Phys. **39** 1993 (2006).
[16] V. S. Raja, Kishore, S. Ranganathan, Bull. Mater. Sci. **9,** 207 (1987).
[17] M. E. McHenry, F. Johnson, H. Okumura, T. Ohkubo, V. R. V. Ramanan, D. E. Laughlin, Scripta. Materialia. **48** 881 (2003).
[18] R. S. Tiwari, N. Mehta, A. Kumar, Chin. J. Phys. **44**(6) 467 **(**2006).
[19] N. J. Christian, Wagner,S. B. Micheal, Mat. Sci. Engg. A. **133,** 26 (1991).
[20] K. Lu, J. T. Wang, Scripta Metallurgica**. 21,** 1185 (1987).

*Corresponding author: mra@cusat.ac.in,
hysenthomas@gmail.com,